Princeton Plasma Physics Laboratory

PPPL-5243

Experimental and modeling uncertainties in the validation of Lower Hybrid Current Drive

F. M. Poli
Princeton Plasma Physics Laboratory, Princeton, NJ, 08543, USA
P. T. Bonoli, M. Chilenski, R. Mumgaard, S. Shiraiwa, G. M. Wallace
Plasma Science and Fusion Center, Cambridge, MA, USA
R. Andre, L. Delgado-Aparicio, S. Scott, J. R. Wilson
Princeton Plasma Physics Laboratory, Princeton, NJ, 08543, USA
R.W. Harvey, Yu.V. Petrov
CompX, P.O.Box 2672, Del Mar, CA 92014-5672, USA
M. Reinke
Oak Ridge National Laboratory, TN, USA
I. Faust, R. Granetz, J. Hughes, J. Rice, J. Walk
Plasma Science and Fusion Center, Cambridge, MA, USA

March 2016

Prepared for the U.S. Department of Energy under Contract DE-AC02-09CH11466.

Princeton Plasma Physics Laboratory
Report Disclaimers

Experimental and modeling uncertainties in the validation of Lower Hybrid Current Drive

F. M. Poli

Princeton Plasma Physics Laboratory, Princeton, NJ, 08543, USA.

E-mail: fpoli@pppl.gov

P. T. Bonoli, M. Chilenski, R. Mumgaard, S. Shiraiwa, G. M. Wallace

Plasma Science and Fusion Center, Cambridge, MA, USA.

R. Andre, L. Delgado-Aparicio, S. Scott, J. R. Wilson

Princeton Plasma Physics Laboratory, Princeton, NJ, 08543, USA.

R.W. Harvey, Yu.V. Petrov

CompX, P.O.Box 2672, Del Mar, CA 92014-5672, USA.

M. Reinke

Oak Ridge National Laboratory, TN, USA

I. Faust, R. Granetz, J. Hughes, J. Rice, J. Walk

Plasma Science and Fusion Center, Cambridge, MA, USA.

Abstract. This work discusses sources of uncertainty in the validation of lower hybrid wave current drive simulations against experiments, by evolving self-consistently the magnetic equilibrium and the heating and current drive profiles, calculated with a combined toroidal ray tracing code and 3D Fokker-Planck solver. The simulations indicate a complex interplay of elements, where uncertainties in the input plasma parameters, in the models and in the transport solver combine and - in some cases - compensate each other. It is concluded that ray-tracing calculations should include a realistic representation of the density and temperature in the region between the confined plasma and the antenna, which is especially important in regimes where the LH waves are weakly damped and undergo multiple reflections from the plasma boundary. It has been found that uncertainties in the processing of the diagnostic data have as large an effect on the calculations as the model approximations. It is shown that by comparing the evolution of the plasma parameters in self-consistent simulations with available data that inconsistencies can be identified and limitations in the models or in the experimental data be assessed.

1. Introduction

Application of radio frequency power in tokamak plasmas in the lower hybrid (LH) range of frequencies has been investigated for nearly three decades. An extensive review of recent progress in LH experiments and in modeling activities is reported in Ref. [1, 2]. Validation of LH models against experiments is challenged by several aspects including, but not limited to, experimental uncertainties in the kinetic plasma profiles and in the equilibrium reconstruction, unresolved measurements at the plasma edge, and a yet incomplete understanding of the LH physics that must be described by the models being validated. The comparison with experiments is complicated by the fact that LH current drive calculations are strongly dependent on the DC electric field, which varies in space and time via poloidal field diffusion in experiments and needs to be calculated and evolved self-consistently with the LHCD [3, 4].

Significant advances in simulation capabilities have been made in order to understand experimental observations [1, 2]. These include development of full-wave solvers to assess the relative importance of diffraction and toroidicity on wave propagation [5, 6, 7, 8, 9], the inclusion of more accurate description of the wave propagation in the plasma edge [4, 10], using realistic plasma profiles and magnetic geometry of the SOL in wave propagation codes [11, 12, 13], the use of coupled ray tracing and 3D Fokker-Planck codes [14, 15, 16]. In particular, the development of combined full-wave/Fokker-Planck models has made it possible for the first time to couple wave propagation calculations in the weak damping regime, using realistic electric field reconstruction in the quasilinear diffusion coefficient. Because of their computational burden, these techniques are being used only for offline analysis on selected time-slices (see, for example, Ref. [5, 7, 17]).

Ray-tracing calculations can instead easily be included in time-dependent calculations, for production runs. Past comparisons of ray tracing and full-wave simulations have even found ray tracing to be valid in weak damping regimes, although work in this area is ongoing [5]. Recently, the ray-tracing code GENRAY [18] has been coupled in TRANSP [19] with the 3D Fokker-Planck solver CQL3D [20] for high fidelity calculations in the lower hybrid range of frequencies. This paper describes the first time-dependent calculations run in TRANSP with GENRAY/CQL3D with a focus on uncertainties in the experimental input data and in the model approximations that can affect the calculations and the validation of LH models against experiments. Several investigations have been conducted prior to this work to compare time-slice simulations with GENRAY/CQL3D to dedicated experiments, in most cases conducting plasma parameters scans on a shot-to-shot basis. Some of these experiments examined fully non-inductive discharges where LHCD was applied for many current relaxation times in a stationary discharge which can then be more accurately diagnosed [8, 14, 15, 22, 23].

Compared to time-slice analysis, validation of Lower Hybrid Current Drive calculations through time-dependent simulations has several advantages. The application of LHCD can affect many aspects of the experimental discharge, such as the

equilibrium shape, the heating, the pressure profiles, the stability, the surface voltage and the current profile. However, without a self-consistent solution many of these observables, such as the current profile, are problematic to compare between model and experiment. Examining solutions without obtaining a self-consistent calculation of these coupled effects could either accentuate or diminish each particular observable agreement with experiment due to the nonlinear interplay between the LHCD and the plasma. This motivates applying a more integrated model to the validation problem. By coupling TRANSP and GENRAY/CQL3D the simulation computes a self-consistent solution that captures the inter-dependencies between the magnetic equilibrium and the current drive model, opening a variety of avenues for comparison instead of comparing only one or two observables.
The evolution in time of simulated quantities, like the current profile, the surface voltage and the Hard X-Ray (HXR) emissivity profile from a synthetic diagnostic in the CQL3D code, can be compared with the corresponding measured quantities: the plasma current reconstructed from MSE pitch angle measurements, the surface voltage and the HXR profiles, as they evolve in time. This integrated approach can unravel inconsistencies between measurements and calculations and identify where improvement to either modeling tools or measurements and/or data reduction is needed. A picture emerges of a complex interplay between diagnostic uncertainties and modeling approximations. Initial results of this validation exercise suggest that - although trends can be identified - no strong claim can be made on the agreement (or disagreement) between measured and calculated quantities for the discharge analyzed, mainly because of the sources of uncertainties in the data analysis and simulation models.

This paper is organized as follows. Section 2-3 introduce the simulation models, the discharge selected for the validation, the diagnostics used for comparison and the experimental observables. Section 4 discusses some of the sources of uncertainty in the validation of models for LH wave physics, such as the local value of Z_{eff} and of the electron temperature, the magnetic equilibrium reconstruction, the edge plasma profiles and the pitch angle measurements. The article then closes with Conclusions and suggestions for future work.

2. TRANSP-GENRAY/CQL3D model and output observables

TRANSP [19] is a time-dependent tokamak transport solver developed at PPPL. The core plasma fluid transport and poloidal field diffusion equations are solved within a time evolving flux surface geometry constructed from a series of axisymmetric MHD equilibrium solutions, with prescribed boundary or using free-boundary solutions. Numerical models and/or input data are provided for heating, momentum, particle and current sources affecting the transport equations. A time step hierarchy is provided so that slowly evolving (and intensive to evaluate) sources are updated as needed, less frequently than every transport time step. The transport equations are formulated over a one dimensional grid with a user chosen time invariant number of radial zones evenly spaced in square root of the normalized enclosed toroidal magnetic flux, with time derivative transformation terms introduced to deal with grid motion (relating normalized flux to actual flux). Source terms are computed over grids optimized for each source model and then interpolated to the transport solver flux grid.

The ray-tracing code GENRAY [18, 24] has recently been coupled in TRANSP with the 3D Fokker-Planck code CQL3D [20] for high-fidelity calculation of LH heating and current drive. The integration and operation mode are illustrated in Fig.1. GENRAY is a generalized 3D optical ray tracing code that integrates the ray equations for the LH waves as they propagate into the plasma. It is coupled with an adjoint calculation for the LH current drive efficiency [25, 26]. GENRAY accounts for the poloidal distribution of the LH waveguide array by distributing rays along the full vertical extent of the launcher. The distributed launch employed in GENRAY is crucial for accurate simulation of the LH wave propagation and absorption since the parallel wavenumber evolution of LH ray trajectories is sensitive to their initial poloidal launch point.
CQL3D is a bounce-averaged Fokker-Planck code. It calculates the flux-surface averaged quasi-linear diffusion coefficient bases on the ray tracing data from GENRAY, and calculates the time-dependent evolution of the electron distribution function resulting from the balance between the LH source, the toroidal electric field, the collisional slowing-down and the pitch angle scattering. The distribution function is solved for in the three dimensions: radius, velocity and pitch-angle.

The integration of TRANSP and GENRAY/CQL3D poses some challenges and opportunities for modeling. The poloidal field diffusion affects the ray trajectories and the evolution of $n_{\|}$, which in turn affects the LH driven current; the DC electric field spatial profile affects the evolution of the electron distribution in CQL3D and thus the LH current drive. The resulting LH driven current then affects the equilibrium, which affects both the poloidal field and the DC electric field profile. Because the plasma is evolving and the current relaxation time is finite, these effects are not separated, but have to be solved self-consistently in a highly integrated time-dependent solution.

With reference to Fig.1, the following approach is taken: at each source time step, the ray data calculated by GENRAY are used in CQL3D to re-calculate the quasi-linear diffusion coefficients. CQL3D distributions are restarted from the previous time step, and CQL3D is sub-time-stepped over the full TRANSP time-step, maintaining consistency of RF absorption and distributions. This calculation uses an internal integration time step in CQL3D, which is then called a number of times necessary to fill-in the separation between successive calls to GENRAY. Thus, if the source time step is 1 ms and the internal integration time in CQL3D is 0.2 ms, CQL3D is called five times. The distribution function is then saved and used at the successive time step. There is an important difference between standalone and time-dependent calculations in this process. In a standalone calculation the distribution function is typically evolved for as long a time as needed to converge the solution. During this time window the pressure profiles and the equilibrium are frozen. In a time-dependent simulation shorter time steps can be taken and the plasma equilibrium and pressure profiles are updated

after each CQL3D cycle of calculations, so that the distribution function is evolved with the plasma.
The LH current calculated by CQL3D is used to evolve the poloidal field diffusion and the procedure is iterated to the successive time step. Since these simulations are using prescribed density and temperature profiles, no transport equations are solved to evolve the pressure profile. TRANSP can be run using a variety of constraints on the equilibrium calculation. For the work reported here the ISOLVER [27] free-boundary equilibrium solver was used to calculate the plasma boundary as it adjusts to heating and current drive, constrained by the measured coil currents. A comparison with the fixed-boundary solution is reported in Sec.4 and indicates that even small differences in the outer boundary can affect the GENRAY/CQL3D solution and the HXR profiles on the outer channels.

As in experiments, where the plasma current waveform is prescribed, the TRANSP simulations discussed in this paper use the plasma current as a boundary condition, leaving the surface voltage unconstrained. The surface voltage is then calculated [27] from the plasma resistivity and the Ohmic current as $V_{loop} = 2\pi R\eta_{\parallel} J^{OH}$, where the plasma resistivity uses the neoclassical NCLASS [48] model and the Ohmic contribution is calculated from the difference between the total current and the non-inductive contribution, which includes the bootstrap current and the LH driven current:

$$J^{OH} = \frac{\langle \mathbf{J} \cdot \mathbf{B} \rangle}{\langle \mathbf{B} \cdot \nabla\varphi \rangle} - \frac{\langle \mathbf{J}^{CD} \cdot \mathbf{B} \rangle}{\langle \mathbf{B} \cdot \nabla\varphi \rangle} \tag{1}$$

The integrated model provides a self-consistent plasma state under the action of GENRAY/CQL3D: the equilibrium and plasma shape, the surface loop voltage, Z_{eff}, pitch angle profile, current profile that can be compared with experimental observables. Also available are the distribution function from CQL3D, the ray trajectories from GENRAY, and hard X-ray bremsstrahlung emission from a synthetic diagnostic in CQL3D.

3. LHCD plasma discharges and observables

Alcator C-Mod [30] is a compact tokamak with toroidal magnetic field up to 8 T, major radius of $R = 0.68$ m and minor radius of $a = 0.23$ m. It is equipped with a LHCD system with source power 3 MW at 4.6 GHz, providing a unique opportunity to test LHCD with the frequency, magnetic field, and density relevant to ITER. The LH launcher is a fully active grill antenna consisting of 4 rows with 15 waveguides per row. The peak $n_{\parallel}$ of the coupled power spectrum can be varied continuously in time from 1.55 to 3.1.

The time traces of the plasma discharge selected for the analysis are shown in Fig.2. This plasma has 0.6 MW of coupled LH power between 0.9 s and 1.8 s. The phasing of the antenna is dynamically changed to decrease the launched $n_{\parallel}$ from 2.5 down to 1.6 in four steps, as indicated in the expanded view of the LH phase in Fig.3. This case study has been chosen for several reasons. First, the step wise change in the launched

$n_\parallel$ of the LH launcher provide discrete perturbations to the plasma system that could more likely produce observable changes to plasma quantities such as loop voltage or HXR emission that are directly affected by the lower hybrid current drive, in much the same way that modulating the RF power level produces changes in the local heating and temperature profiles. However the interplay between observable quantities is known to be complex. First, the conditions for LH damping and penetration do change with $n_\parallel$ and so does the current drive efficiency. With decreasing $n_\parallel$ the waves are expected to penetrate deeper into the plasma and to be absorbed at smaller radial locations, where the electron temperature is higher and more easily satisfies the condition for quasilinear electron Landau damping given by [28] $T_e \simeq 41 n_\parallel^{-2}$, with temperature in keV.

Since the current drive efficiency is inversely proportional to $(n_\parallel)^2$ [34] an increase in the driven current should be observed with decreasing $n_\parallel$. On the other hand, the condition for adequate LH wave accessibility ($n_\parallel > n_{acc}$) is not as well satisfied as $n_\parallel$ is reduced during the phasing scan, where n_{acc} is given by [29]:

$$n_{acc} = \frac{\omega_{pe}}{\omega_{ce}} + \left[1 + \left(\frac{\omega_{pe}}{\omega_{ce}}\right)^2 - \left(\frac{\omega_{pi}}{\omega}\right)^2\right]^{1/2}, \qquad (2)$$

where $\omega_{pe,pi}$ is the plasma frequency for electrons and for ions respectively and ω_{ce} is the electron cyclotron frequency. Thus, refractive effects associated with reduced wave accessibility can impede the wave penetration expected at lower $n_\parallel$ due to quasilinear penetration to higher electron temperature.

Conversely, at higher values of $n_\parallel$, the wave should be absorbed via electron Landau damping at lower electron temperatures (see above) causing the absorption to move out radially. Furthermore, since the absorption in C-Mod is in the weak damping regime where multiple reflections of the wave can occur, especially for $n_\parallel$ between 1.6 and 2.2, the analysis of this case provides a challenge for the accuracy of the edge / SOL model.

It should be noted that the line averaged density monotonically decreases during the LH phase resulting in an increase in the current drive efficiency [34], thus the effect of density and $n_\parallel$ cannot be completely separated.

A further complication is that for all four $n_\parallel$ values in the range of 1.6 to 2.5 the waves are only weakly absorbed because they do not satisfy the condition for strong quasilinear damping; thus the interplays described here which are based on a strong single pass damping picture can be significantly modified. In addition it will be important to have accurate density and temperature profiles near the last closed flux surface and in the scrape-off layer (SOL) as well as accurate magnetic equilibrium reconstructions in the SOL since this will affect the LH wave physics as it undergoes multiple radial reflections from the edge. Finally, this discharge is not fully non-inductive and has not reached steady-state, which implies the DC electric field has a non-negligible contribution in the LH calculations. This is therefore a good test to assess the robustness of the calculations in a time-dependent loop where the equilibrium is evolved self-consistently with the LH heating and current profiles.

3.1. Gaussian Process Regression and the kinetic plasma profiles

Figure 4 shows the density and temperature profiles from the Thomson scattering diagnostic during the Ohmic phase and in four time windows during the LH phase, corresponding to the different values of $n_{\parallel}$, as indicated. The profiles are fitted using a Gaussian Process Regression (GPR) technique [35]. Experimental data are fitted over sliding time windows, with 10 ms separation and averaged over 40 ms. Compared to standard spline fitting, this technique has proven to deliver statistically rigorous fits and better uncertainty estimates for both the local value and the gradient of plasma profiles with an improved level of automation [36]. However, LH discharges present particular challenges to the fit of temperature profiles, because the localized power deposition at mid-radius causes bumps in the profiles that are not always captured in the GPR fit. As shown in the figure, the fit tends to underestimate the electron temperature at mid-radius, at the location where the LH primarily deposits. We also notice the high density of data at the edge, which increases uncertainties in the characterization of the edge temperature and density and therefore in the calculations of the LH damping. Since the model for the Scrape-Off-Layer plasma in GENRAY uses the values of density and temperature at the edge to unfold the profiles outside the separatrix, uncertainties in these values are reflected in the SOL plasma profiles.

3.2. Hard X-ray camera

Electron Landau damping generates a fast electron population that emits bremsstrahlung radiation in the Hard X-Ray (HXR) region of the spectrum. On C-Mod, a pinhole camera consisting of an array of 32 CdZnTe detectors is used to image energies in the range of $[20, 200]$ keV (see Fig.5) [37]. The spatial resolution of the diagnostic is about 1.4-1.7 cm. Since the local emissivity depends on the location of the damping, HXR measurements represent a simple and direct observable of LHRF generated fast electron physics. Combined with a synthetic diagnostic with a model distribution function, HXR measurements do provide a means for validation of LH calculations. The CQL3D Fokker-Planck solver [20] is used to compute a fast (non-thermal) electron distribution generated by the LHRF power. This is then used in a synthetic diagnostic that takes into account the bremsstrahlung emission cross-section, the viewing geometry, the detector response function, and the presence of any absorber such as a vacuum window, and calculates the expected chord-integrated spectra. Thus a comparison of the simulated and measured chord-integrated HXR spectra provides a consistency check on the height and width of the quasilinear plateau and the spatial localization of the fast electron population. The profiles shown herein do represent line integrated measurements with no inversion based on the equilibrium. This eliminates uncertainties due to the accuracy in the equilibrium reconstruction.

3.3. Motional Stark effect constrained equilibrium

C-Mod is equipped with a Motional Stark effect diagnostic (MSE) that observes the polarization of the Doppler-shifted Balmer-α emission from a 50 keV Hydrogen Neutral Beam [38]. The system comprises ten channels covering radii between 0.69 m and 0.86 m. Due to the size of the neutral beam and the geometry of the view, each MSE sightline averages the polarized emission over a radial portion of the plasma. The averaging decreases (improves) from 5.3 cm in the core down to 1.17 cm at the edge. Due to the pulsing of the beam there are sixteen time windows where MSE measurements are available in this discharge, and they are indicated in Fig.3 as horizontal lines. To ensure adequate photon statistics the integration time of the MSE is the majority of a beam pulse, about 60 ms, with a MSE measurement available every 100ms from plasma ramp-up thru ramp-down. For comparison, the current relaxation time during the LH heated phase in the discharge analyzed herein is $\tau_{CR} = 287$ ms. This has been calculated as $\tau_{CR} = 1.4a^2\kappa T_e^{1.5}Z_{eff}^{-1}$, using average values during the LH phase: $T_e(0) = 3.5$ keV, $Z_{eff} = 2.7$, $\kappa = 1.6$. Thus the equilibrium can evolve within a MSE measurement. In the discharge examined in this paper the time between successive changes in the launched $n_{\|}$ was over 200ms and the MSE time period of interest is taken to be in the latter half of the window to allow as much time for the equilibrium to evolve toward a new state prior to acquiring the measurement. At the time of the experiment, the MSE system experienced a small ($< 0.5°$) shot-to-shot additive offset drift attributed to stress-induced birefringence in in-vessel lenses. This drift is well understood, was constant within a discharge [23], and has since been eliminated. This small offset precludes direct use of the measured pitch angles to constrain the magnetic equilibrium. Instead, an in situ calibration is constructed by comparing the measured pitch angle to that calculated from EFIT constrained by kinetic profiles, $q_0 = 0.9$ and $q = 1$ at the sawtooth inversion radius during the long Ohmic phase of the plasma prior to the LHCD, but 400ms after plasma flattop [42]. This results in a channel dependent angular offset that is applied to the other parts of the discharge. Two Ohmic periods are provided in this shot for this purpose (t=0.76s and t=0.86s) and the equilibrium is no longer evolving immediately prior to or during these periods. The resulting offset is shown to be small and similar to offsets in other shots that day. This procedure has been verified using long steady Ohmic discharges, discharges with LHCD that have long Ohmic periods prior to and after the LHCD period [23], and using specialized MSE calibration discharges [43]. However, it does depend on q-profile constraints in the Ohmic period. The MSE measurements are incorporated into an equilibrium reconstruction along with other measurements in a process called MK-EFIT centered at each MSE measurement window [44]. Four-knot splines are used for FF' and P' basis functions in EFIT [40] to allow flexibility to describe different internal profiles and increasing the number of knots is not shown to improve the resulting equilibrium. Here F and F' are respectively the toroidal flux function and its derivative with respect to poloidal flux, and P' is the derivative of pressure with respect to poloidal flux.

Temperature and density profiles from Thomson scattering are combined with an estimated ion temperature profile from neutron rate and Z_{eff} to produce a pressure profile which is averaged over the MSE time resolution and GPR processed and used as a constraint. The MSE pitch angle is combined with the location of the magnetic axis from Shafranov shift calculation and the pitch angle at the limiter from magnetics. The resulting pitch angle profile is also GPR processed to produce a denser interpolation over twenty points that only spans the MSE measurement range. The use of the interpolation via GPR prevents the solution from being overly sensitive to the details of the spline knot locations and tensions and is warranted since - by construction - EFIT must produce smoothly varying profiles. The resulting equilibrium thus combines a variety of diagnostics including kinetic profiles, magnetic pick up coils, flux loops, coil currents, and MSE in a self-consistent manner commiserate with the individual measurement uncertainties. The addition of the MSE and kinetic data to a magnetics-only EFIT is shown to only marginally increase the total χ^2 and results in a significantly different current profile but nearly identical plasma shape. This is indicative of the MSE and kinetic measurements being consistent with the magnetics data outside the plasma. In the discharge of interest the resulting MK-EFIT shows q_0 going above unity during the LHCD phase when sawteeth disappear and returning to below unity when sawteeth reappear after LHCD. The maximum q_0 observed remains below 1.2. All the inputs are then varied in a Monte Carlo manner within their uncertainties, re-fit, and reanalyzed by EFIT to produce uncertainty estimates.

4. Effect of uncertainties in the model and experiments

In a validation effort it is important to keep track of the various sources of uncertainty. As the model becomes more integrated and representative, the monitoring of how uncertainties propagate is even more important, since the various components interact non-linearly. The integrated model also allows one to compare a wider variety of observables between the experiment and the simulation in a comprehensive manner. Uncertainties in the validation of the LH models come from, but are not limited to (a) convergence of the distribution function calculations (b) uncertainties in the LH model itself (c) uncertainties in the plasma parameters that are input to the LH model (d) uncertainties in the equilibrium reconstruction output as well as (e) uncertainties in the equilibrium solver in the time-dependent simulations.

4.1. Uncertainties due to the local value of Z_{eff}

C-Mod has a single chord visible bremsstrahlung measurement observing the plasma in the toroidal midplane, with a tangency radius near the axis. This diagnostic is absolutely calibrated and can produce chord integrated Z_{eff} measurements from the following equation:

$$Z_{eff} = 1.68 \times 10^9 \; ds \; n_e(s)^2 T_e(s)^{-0.353} \; [10^{20}\mathrm{m}^{-3}, \mathrm{keV}] \tag{3}$$

To obtain Z_{eff} from the visible bremsstrahlung measurement the temperature and density profiles must be properly accounted for. On C-Mod this is typically done using the line-integrated density and temperature measurements from an Electron Cyclotron Emission (ECE) diagnostic. However, during LHCD the latter is contaminated with non-thermal electrons making this analysis incorrect. The Z_{eff} calculated this way assuming a flat profile is shown in Fig.7 (blue curve).

Since the local LH current drive efficiency is proportional to $(5 + Z_{eff})^{-1}$, it is expected that assuming a flat rather than a peaked profile does make a difference. A profile of Z_{eff} that is consistent with the measured radiation and that falls within the range of values estimated from Eq.3 is obtained as follows. The profiles of high-Z impurities are inferred from the measured radiation using:

$$P_{rad} = \sum n_i n_e L_i(T_e) \tag{4}$$

where the index i runs over all impurity species, $L_i(T_e)$ is the cooling rate for each impurity and is a function of the electron temperature (see Fig.6), n_i and n_e are the impurity and electron density respectively. In addition to molybdenum, always present in C-Mod plasmas, argon is injected in this discharge at about 0.2 s, although no calibrated measurements are available. Light-Z impurities are assumed to be a constant fraction of the electron density, in time and radius. Based on average values on C-Mod, it is assumed here that boron is 1% of the electron density and oxygen, always present in the discharge, is about 1/3 of boron. With these assumptions, an upper limit to the argon fraction is taken to be $n_{Ar}/n_e = 10^{-3}$, by imposing quasi-neutrality and that the Z_{eff} does not exceed the value calculated from Eq.3. The profile of argon is assumed to be the same as the electron density profile and the profile of molybdenum is calculated from Eq.4. Simulations run with more peaked argon profiles results in negligible differences and do not change the conclusions of the analysis. The impurity profiles, estimated this way, are used in TRANSP to calculate Z_{eff} and the radiation profiles. Despite the approximations made to infer the profile of Z_{eff}, the central value calculated this way is in good agreement with the estimate from Eq.3, as shown in Fig.7 (red curve). Since the radiation is dominated by molybdenum, the calculated profiles are also in good, qualitative agreement with the bolometer measurements. Deviations from the measured profiles are likely caused by a more sophisticated model used in TRANSP, compared to Eq.4.

Figure 8 compares two TRANSP simulations, one run with Z_{eff} calculated in TRANSP from impurity profiles and one with flat Z_{eff} profile, as calculated from Eq.3. The simulation that uses a Z_{eff} profile (red curves) results in better agreement with the surface voltage during the LH phase and in the prior ohmic phase; both simulations overestimate V_{loop} after the LH phase, where the argon concentration and Z_{eff} are likely overestimated. The better agreement during the ohmic phase can likely be attributed to a combination of profile shaping and amplitude, while during the LH phase, where the Z_{eff} in the center is comparable, the better agreement is likely a consequence of using a peaked rather than a flat profile.

It is important to note that the LH current density profiles are comparable within uncertainties over most of the radial region, except perhaps during phase I, while the HXR profiles are very sensitive to the local value of Z_{eff}. Simulations with a flat profile result in a broader HXR profiles and increased count rate over the outer channels, in better agreement with measurements during phases I ($n_\parallel = 2.5$) and II ($n_\parallel = 2.2$). However, a peaked Z_{eff} profile results in better agreement with the number of photon counts in the central channels during phase III and IV, despite the LH current profiles being very similar. These results indicate that accounting for local variations in the Z_{eff} in the propagation and damping of LH waves is important and that the HXR diagnostic is a very sensitive observable to assess the uncertainties in the input profiles. The sensitivity of the hard X-ray profiles on the details of the Z_{eff} profile could be a consequence of the fact that the emission detected by the horizontally viewing HXR camera depends on the pitch angle scattering of electrons from the parallel to the perpendicular directions, which is a direct function of Z_{eff}. In this respect it may be that both a horizontally viewing and tangentially viewing HXR diagnostic are desirable.

Another interesting observation is that the measured V_{loop} is not a sensitive indicator of the effect of Z_{eff} on LH current drive, at least not as sensitive as the HXR profiles. As described in the previous Sec.2, the surface voltage is calculated in TRANSP from the plasma resistivity and from the Ohmic current as $V_{loop} = 2\pi R\eta_\parallel J^{OH}$. Although the ohmic current is not calculated explicitly from resistivity, the contribution from the Z_{eff} and T_e profiles is hidden in the current drive term J^{CD} and it cannot easily be separated. While the surface voltage alone is not a sensitive indicator of the accuracy of the LH model, it is still a good indicator of the self-consistency of the solution, when examined together with other observables.

4.2. Uncertainties due to the magnetic equilibrium solver

Figure 9 compares free-boundary (with ISOLVER) and fixed-boundary (with TEQ) calculations. The simulations use the same Z_{eff} profile and the same plasma density and temperature profiles.

Both simulations exhibit a good agreement with the measured surface voltage. The integrated LH driven current is comparable in the two cases, except during phase II, where the fix-boundary calculations predict a larger driven LH current. During this phase the LH current density profiles are significantly different in the inside mid-radius, with the fixed-boundary calculations resulting in more current density in the core and larger number of simulated photon counts in the core channels. Figure 9 compares the plasma boundary taken from EFIT and the plasma boundary reconstructed with ISOLVER using the measured coil currents at 1.36 s. The outer boundary is shifted inward and the X-point location is higher in the free-boundary calculations. Also, magnetic surfaces outside the separatrix are displaced. Despite the fact that the fixed and free boundary equilibria are quite close inside the separatrix, it is clear that even small differences in the magnetic equilibrium calculations - especially in the SOL and in the plasma boundary - can result in significant differences on the ray propagation and on the LH current profiles (see Fig.9d-d$'$) as well as uncertainties in the HXR emissivity profiles.

4.3. Uncertainties due to the edge plasma profiles

In regimes like C-Mod, where the LH waves undergo multiple reflections inside the vessel before being completely absorbed, accurate modeling of the plasma between the antenna and the last closed flux surface becomes critical [13]. The simulations discussed in the previous sections use a simple SOL model in GENRAY. The temperature and density profiles in the SOL are determined by an e-folding width λ based on the distance from any point to the LCFS. The normalized e-folding width, $\sigma \equiv \lambda/a$ where a is the plasma minor radius, is a fixed value for all poloidal angles ($\sigma_T = 0.05$) for the temperature, while it is a function of poloidal angle for the density. The SOL density profile is narrowest near the HFS mid-plane ($\sigma_n = 0.023$), wider on the LFS mid-plane ($\sigma_n = 0.046$), and widest in the divertor regions ($\sigma_n = 0.09$). The ray equations are integrated by GENRAY in the same manner as inside the LCFS, including the magnetic equilibrium generated by TRANSP. Landau damping of the rays outside the LCFS is not calculated by CQL3D, however collisional absorption in the SOL calculated by GENRAY is passed to CQL3D and included in the overall power accounting.

Figure 11 compares two simulations, one with a SOL as described above and one with a very narrow SOL, so that the ray trajectories are reflected immediately outside the separatrix. This case is referred to as ‘no SOL’ in the figure. The two assumptions in GENRAY result in significantly different current profiles and HXR profiles, depending on the value of $n_\parallel$. When a SOL is included in the calculations the LH waves can propagate and undergo multiple reflections, depositing energy in the region between the plasma and the antenna. As shown in Fig.11, the case with a narrow SOL displays almost no current in the peripheral plasma, except at the lowest value of $n_\parallel$. Since no power is deposited via collisions in the outer region, beyond the last closed flux surface, the rays undergo a larger number of reflections inside the separatrix before the entire power is absorbed. This explains why the LH current density in the core is larger in the case of narrow SOL. With decreasing $n_\parallel$ the waves naturally propagate deeper inside, reflections in the edge plasma region are less important and differences in the current density profiles in the core become smaller. The amplitude of the HXR emissivity from the synthetic diagnostic becomes thus comparable.

This comparison is interesting for two reasons: first, it indicates that the edge plasma conditions are important for the correct calculation and interpretation of the ray propagation; second, it confirms how the HXR profiles are a sensitive diagnostic of the LH model and of the consistency of the plasma input parameters. The V_{loop} is instead an observable that depends on the nonlinear interaction between the current profiles, the magnetic equilibrium and the pressure profiles, whose effects cannot be separated from each others. Thus, for example, no conclusion can be drawn from the sole comparison of the integrated LH current and the V_{loop} as of whether the SOL model used is accurate, an issue already addressed in Sec.4.1 in the case of the Z_{eff}.

Recent work [13] addressed parasitic absorption via collisional damping in the edge plasma by including more realistic temperature and density profiles in diverted geometry. This is done using a two-point model, where the temperature and density measured at the outer midplane and in the divertor region are used to reconstruct 2D density and temperature profiles by assuming constant pressure along open field lines. This model provides a more accurate description of the collisional absorption in the plasma edge and should routinely be used in the GENRAY/CQL3D calculations.

4.4. Uncertainties due to the local value of electron temperature

The LH current drive efficiency is directly proportional to the local value of the electron temperature and inversely proportional to the density. Furthermore, in weak damping regimes like on C-Mod, where the rays undergo multiple refections before the LH power is absorbed, small variations in the local density and temperature profiles might be expected to result in significantly different profiles of LH current density and power absorption. Somewhat paradoxically this is not necessarily the case. This is because the ray equations in toroidal geometry have been shown formally to be a stochastic system that is most evident in weak damping regimes [39]. The consequence of this ray stochasticity is that a weakly damped ray can fill an entire phase space (x, k) that locally spans wavenumbers extending from the LH wave accessibility limit to phase velocities where strong electron Landau damping occurs. In this case local variations in the profiles of plasma density and temperature become less important. Nonetheless we have performed simulations where the local electron temperature has been varied to partially test this hypothesis, by allowing variations in the fitted profile so that the temperature is lowered on the inside mid-radius and raised on the outside mid-radius by approximately 10%. Results are shown in Fig.12 for phase I-II in the first case, since the second case results in a large overdriven current, indicating that - even though still within the large diagnostic uncertainties, these variations are inconsistent with the evolution of the measured observable. No differences is seen during phase III-IV, when $n_{\parallel} < 2$ and these profiles are not shown in the figure.

Despite of the differences in the local temperature in the outer region, the differences in the HXR profile emissivity in the outer channels are smaller than differences that are caused from local variations in the Z_{eff}, from the plasma boundary position or from assumptions on the SOL width, as discussed in the previous sections. Differences in the core channels are instead larger, although they appear to be uncorrelated to the lower values of the electron temperature. In fact, in both time windows the electron temperature has been reduced in the core, but the HXR counts are larger during phase I and lower during phase II. This comparison seem to indicate once again that the HXR emissivity profile is a sensitive observable, but that there is no evident trend with local variations in the electron temperature in the core plasma.

4.5. Uncertainties due to the fast electron radial diffusion

The CQL3D code solves a model electron equation of the form [21]:

$$\frac{\partial}{\partial p_\parallel} D_{rf}(p_\parallel)\frac{\partial f_e}{\partial p_\parallel} + C(f_e, p_\parallel, p_\perp) + eE_\parallel \frac{\partial f_e}{\partial p_\parallel} + \Gamma_s \delta(p_\parallel) + \frac{1}{r}\frac{\partial}{\partial r} r\chi_f \frac{\partial f_e}{\partial r} = \frac{\partial f_e}{\partial t} \quad (5)$$

where f_e is the electron distribution function, D_{rf} is the quasi-linear RF operator, $C(f_e, p_\parallel, p_\perp)$ the collision operator in 2D velocity space that includes the effects of particle trapping as well as momentum-conserving corrections, $E_\parallel$ the DC electric field, and χ_f the fast electron diffusion term. Fast electron diffusion in velocity space introduces an uncertainty because it affects the electron tail and therefore the absorption of the LH waves, their radial penetration and the amplitude of the driven current. A model form for the fast electron diffusivity is taken to be [46]:

$$\chi_f = \chi_0 \frac{(v_\parallel / v_{te})}{\gamma^3}, \text{with } \gamma^2 = (1 - v^2/c^2)^{-1} \quad (6)$$

The diffusion coefficient χ_0 has been determined to be in the range of $[0.01, 0.04]$ m^2/s on Alcator C-Mod using a LH modulation technique [47, 15]. Comparable values had been previously determined independently by matching the HXR synthetic diagnostic in CQL3D with measurements [14]. In the absence of a direct estimate of the radial diffusion, the procedure was to vary the coefficient χ_0 in the CQL3D calculations until the HXR synthetic diagnostic and the experimental HXR profiles agree with each other.

Figure 13 compares time-dependent simulations run with three assumptions on the value of χ_0, namely $\chi_0 = 0.0, 0.01, 0.05$ m^2/s. The case with no radial diffusion is the same shown in Fig.9 (green curve) and in Fig.11 (blue curve). Figure 14 compares the profiles of plasma current density and of the safety factor for the same cases with the profiles from the EFIT reconstruction constrained by the MSE diagnostic (black curve). The effect of a non-zero radial diffusion term is to increase the LH current in the core, as shown in Fig.13, where the LH current profiles change from hollow to almost flat with increasing magnitude of χ_0. This discharge is not fully non-inductive and a non-negligible ohmic contribution is still present during the LH phase. With a requested current of 0.6 MA and a LH driven current that increases from about 0.3 MA to 0.5 MA, the inductive current contributes up to 50% of the total current during the early LH phases I-II. TRANSP simulations, similar to experiments, are run to keep the total current constant and this condition is satisfied by compensating for the missing current with an inductive current, which is driven predominantly in the core. This explains why the simulated plasma current profiles are monotonic during phase I-II, when the inductive current is comparable to the non-inductive contribution (see Figs.13-c and 13-f). It is noted that $\chi_0 = 0.05$ m^2/s is the value needed for the calculated current density profiles to agree with the current reconstructed from the MSE pitch angle measurements, in particular during phase III and IV. This value is close to the range of $\chi_0 = 0.01 - 0.04$ m^2/s derived from experiments with LH power modulation [47, 15] and to the value of $\chi_0 = 0.04$ m^2/s inferred from a comparison with HXR emission and with the total current in experiments with fully non-inductive current drive [14, 47, 15]. The larger value of χ_0 also ensures the best agreement with the magnitude of the measured HXR emissivity profiles along the central chords in all phases, although the calculated profiles are too peaked.

It should be noted that sawteeth are present in this discharge during the ohmic phase and during part of phase I. The sawtooth period is nevertheless very small and calculations run in TRANSP with a predictive sawtooth model turned-on are not affected by the model. For this reason, all simulations are run without accounting for the effect of sawteeth in the evolution of the equilibrium.

Figure 15 shows the pitch angle measurements (blue symbol) from the MSE diagnostic. The point at 90 cm is from magnetic measurements and it is used to constrain the calculations in EFIT. The horizontal lines in the figure indicate the radial measurement region of the MSE, whose size decreases from 5.3 cm to 1.17 cm moving from the innermost to the outermost channel. They are in a different color to be distinguished from the experimental error bars. The MSE measurements, available at ten radial locations, are interpolated over twenty radial locations using Gaussian Process Regression (GPR) for each time slice (black points in the figure). For comparison, the pitch angle calculated from the TRANSP free boundary simulation with $\chi_0 = 0.05$ m$^2/s$ (green shaded area) is also shown. Here the simulated pitch angle has been averaged over 60 ms and the thickness of the shaded area indicates the standard deviation with respect to the average value. The agreement between the measured and the simulated pitch angle is very good during phase I-II, but differences increase during phase III-IV in the outer mid-radius. During these phases the pitch angle calculated in the case of $\chi_0 = 0.01$ m^2/s is also shown (red shaded area). With reference to Fig.13 these two cases result in a current and safety factor profile that are consistent within uncertainties with the profiles inferred from MSE pitch angle measurements.

4.6. Uncertainties due to the model numerics

The convergence of the distribution function can be affected by the mesh resolution in the velocity space, the integration time and the number of time steps in the CQL3D calculations between two successive calls to GENRAY. A rigorous procedure for Uncertainty Quantification should take into account these variations, together with every variation in the input profiles. For the discharge analyzed herein, simulations have been run for a fixed set of input parameters and profiles and for $\chi_0 = 0$. The number of mesh points in the velocity space has been varied between 340 and 600. It is found that increasing the number of mesh points above 300 leads to better convergence, especially in the case of lower $n_\parallel$. This discharge, where the $n_\parallel$ is changed during the LH duration, is therefore an ideal case to test the robustness of the implementation of CQL3D in TRANSP. In this scan the internal integration time in CQL3D has been varied between 0.1 ms and 1.0 ms, and the number of steps between two successive calls to GENRAY from 5 to 10, which corresponds to time steps of 1 to 5 ms. The results of this scan are shown in Fig.16. The shaded area indicates the maximum range of variation for different choices of the above parameters in four time windows, corresponding to the four values of parallel wavenumber, averaged over 60 ms, the integration time of the MSE diagnostic. The uncertainties depend on the plasma conditions and on the value of $n_\parallel$. For comparison, the figure also shows the average value in the same time window of calculations done with 400 mesh points in the velocity space, 0.4 ms internal integration time step in CQL3D and 2 ms between successive calls to GENRAY in TRANSP. We notice that, for all values of $n_\parallel$, the standard deviation of the calculated LH current in a single time window of 60ms is smaller than the range of variation caused by the input parameters used in the GENRAY-CQL3D calculations. In particular, the variations in the output are large during phase II at all radii and during phase IV in the outer mid-radius. These variations could reconcile some of the discrepancies observed at large radii in this phase, for example in the simulated pitch angle.

5. Conclusions

Validation of lower hybrid wave current drive simulations against experiments offers several challenges. First, the physics of LH wave absorption in weak damping regimes is not entirely understood [1]. Second, the models used have intrinsic limitations and rely on approximations. This includes the need for use of reduced models in time-dependent calculations to save computational time, such as the use of ray tracing calculations as opposed to full-wave electromagnetic field simulations. Third, experimental uncertainties in the plasma kinetic profiles and in the equilibrium reconstruction that are input to the LH codes introduce errors in the calculations, affecting the ray propagation and the wave damping. Recently, the ray-tracing code GENRAY and the Fokker-Planck solver CQL3D have been implemented and coupled in TRANSP for high-fidelity calculation of LH heating and current drive. By solving self-consistently the evolution of the magnetic equilibrium, the calculation of the LH heating and current drive takes into account the diffusion of the poloidal field. The profile and magnitude of the DC electric field, which is a critical element in the calculation of the LH current, is calculated from a self-consistent solution of the poloidal field diffusion equation, without the need to assume that the discharge has reached steady state where the electric field profile can be assumed to be spatially constant. The latter hypothesis fails in particular when a residual ohmic current is left.

The simulations indicate evidence of a complex interplay of elements, where uncertainties in the input plasma parameters, in the LH model and in the transport solver combine and - in some cases - compensate each other. Ray-tracing is an initial value problem and results do depend on the initial conditions. Small shifts in the outer boundary and in the X-point result in ray trajectories, driven LH current density profiles, and HXR emissivity profiles that can vary significantly. This is a consequence of the fact that the ray equations exhibit stochasticity in the weak damping limit [39]. Furthermore, in regimes of multi-pass absorption, like on C-Mod, it is expected that ray trajectories undergo several reflections from cut-offs, limiters, or the vessel wall, which are treated as ideal in ray-tracing codes. A direct consequence is that the modeling of the plasma edge is critical in the calculation of the ray-trajectories. Extensive efforts now exist to develop more accurate models for the SOL in ray tracing calculations by employing edge measurements of density and temperature in open field geometries [13]. However, results from ray-tracing analysis should be routinely compared with full wave analysis, where the wave propagation in the region between the antenna and the plasma is modeled more accurately, including the proper treatment of wave reflection at cut-off layers and caustics, for example.

The HXR emissivity profile is a sensible observable of the LH propagation and responds to local variations of the Z_{eff}, while the surface voltage is affected by the nonlinear interaction of the plasma equilibrium, the LH current density, the plasma resistivity and the pressure profiles. However, while the V_{loop} alone cannot be used as a criterion to discriminate between models, the comparison of the V_{loop} and other plasma observables together is a valuable mean of assessing the self-consistency of the model used and of the input profiles. A new Visible Bremsstrahlung diagnostic has been installed in C-Mod for measurement of Z_{eff} profiles during the time of writing, which is going to provide an additional, important feedback control in TRANSP for validation of LH models.

An important conclusion from this work is that validation of lower hybrid models must take into account a variety of effects which can all work to influence the final comparison with a single diagnostic such as hard X-ray emissivity for example. It is by comparing the evolution of the various parameters in simulations and experiments that inconsistencies can be identified and limitations in the models or in the experimental data can be addressed.

Acknowledgments

This work was supported by the US Department of Energy under contract DE-AC02-CH0911466 and under Contract No. DE-FC02-99ER54512 on Alcator C-Mod, a Department of Energy Office of Science User Facility.

References

[1] P.T. Bonoli *Phys Plasmas* 2014 **21** 061508
[2] Y. Peysson, J. Decker, E. Nilsson, J-F Artaud, A. Ekedahl, M. Goniche, J. Hillairet, B. Ding, M. Li, P.T. Bonoli, S. Shiraiwa, M. Madi, *Advances in Modeling of Lower Hybrid Current Drive*, accepted for publication in Plasma Phys. Controlled Fusion.
[3] Y. Peysson and J. Decker, Fusion Sci. Technology **65** 22 (2014)
[4] E. Barbato, A. Savaliev, I. Voitsekovitch, K. Kirov, M. Goniche, the ISM ITER Scenarios MOdeling group and JET-EFDA contributors, Nucl. Fusion **54** 123009 (2014)
[5] Wright J.C. *et al* (2009) Phys. Plasmas **16** 072502
[6] Meneghini O. *et al* Phys. Plasmas (2009) **16** 090701
[7] S. Shiraiwa *et al* Phys. Plasmas (2010) **17** 056119
[8] S. Shiraiwa *et al* Phys. Plasmas (2011) **18** 080705

[9] Meneghini O. *et al* Fusion Sci. Technol. (2011) **60** 40
[10] J. Decker, Y. Peysson, J-F Artaud, E. Nilsson, A. Ekedahl, M. Goniche, J. Hillairet, and D. Mazon, Phys. Plasmas **21** 092504 (2014)
[11] Wallace G.M. *et al* (2010) Phys. Plasmas **17** 082508
[12] O. Meneghini, *Full wave modeling of lower hybrid waves on Alcator C-Mod*, Doctoral Thesis, Department of Nuclear Science and Engineering, Massachusetts Institute of Technology (February, 2012).
[13] S. Shiraiwa, 21st Topical Conference on Radiofrequency Power in Plasmas, Lake Arrowhead, CA (April 27-29, 2015) Invited Paper I2; (AIP Conference Proceedings XXXX, AIP, NY (2015).
[14] P.T. Bonoli, J. Ko, R.R. Parker, A.E. Schmidt, G. Wallace, J.C. Wright, C.L. Fiore, A.E. Hubbard, J. Irby, E. Marmar, M. Porkolab, D. Terry, S.M. Wolfe, S.J. Wukitch, the Alcator C-Mod, J. R. Wilson, S. Scott, E. Valeo, C.K. Phillips and R.W. Harvey, Phys. Plasmas **15** 056117 (2008)
[15] A.E. Schmidt, P.T. Bonoli, O. Meneghini, R.R. Parker, M. Porkolab, S. Shiraiwa, G. Wallace and J.C. Wright, Phys. Plasmas **18** 056122 (2011)
[16] Y. Peysson, J. Decker, and L. Morini, Plasma Phys. Controlled Fusion **54** 045003 (2012)
[17] C Yang, *et al*, Plasma Phys. Control. Fusion **56** (2014) 125003
[18] A.P. Smirnov and R.W. Harvey, Bull. Amer. Phys. Soc. Vol. 40, No. 11, p. 1837, Abstract 8P35 (1995); CompX report CompX-2000-01 (2001). See http://www.compxco.com/genray.html
[19] Hawryluk R.J., An empirical approach to tokamak transport. In B. Coppi *et al*, editor, *Physics close to thermonuclear conditions* **1**, 19, Brussels, 1980. Commission of the European Communities.
[20] Harvey R.W. and McCoy M.G. (1993) in *Proceedings of the IAEA Technical committee on Advances in Simulation and modellng of Thermonuclear plasmas*, 489, Vienna, IAEA
[21] R.W. Harvey, O. Sauter, R. Prater, and P. Nikkola, *Phys. Rev. Lett.* **88**, 205001 (2002)
[22] T.T. Mumgaard, S.D. Scott, S. Shiraiwa, G.M. Wallace, R.R. Parker, J.W. Hughes, R.S. Granetz, *Measurement of the current profile in Alcator C-Mod with lower hybrid current drive using an upgraded motional Stark effect diagnostic, AIP Conference Proceedings 1680, 394 (2014)*
[23] R. T. Mumgaard, Lower Hybird current drive on Alcator C-Mod: measurements with an Upgraded MSE diagnostic and comparison to Simulations, PhD Thesis, Massachussets Institute of Technology (2015)
[24] Smirnov A.P. *et al*, (2009) In *Proceedings of the 15th Workshop on ECE and ECRH*, 301. World scientific.
[25] Karney C.F.F. and Fisch N.J., (1985) *Phys. Plasmas* **28** 116.
[26] Karney C.F.F., Fisch N.J. and Reiman A.H., In R. McWilliams, editor, *Radio-Frequency power in plasmas*, (1989) **190**, page 430, New York, AIP Conf. Proc.
[27] R. Andre, TRANSP Isolver free boundary equilbrium solver, Bulletin of the American Physics Society, APS-DPP 2012
[28] Brambilla, M., Ignition with lower hybrid heating, in Physics of Plasmas Close to Thermonuclear Conditions (Brussels, Commission of the European Communities, 1980), Vol. I, pp. 291311.
[29] Brambilla, M., Waveguide launching of lower hybrid waves", Nuclear Fusion 19, 13431357 (1979).
[30] Hutchinson I.H., Boivin R., Bombarda F. *et al*, (1994) *Phys. Plasmas* **1** 1511.
[31] P. T. Bonoli et al, Fusion Science and Technology, Volume **51** (2007) 401-436
[32] S. Shiraiwa et al (2011) Nucl. Fusion **51** 103024
[33] G.M. Wallace et al (2013) Nucl. Fusion **53** 073012
[34] Fisch N.J, Rev. Mod. Phys. (1987) **59** 175
[35] Rasmussen C.E. and Williams C.K.I.. *Gaussian Processes for Machine Learning.* MIT Press, 2006.
[36] Chilenski M.A. *et al* (2015) *Nucl. Fusion* **55** 023012
[37] J. Liptac, R. PArker, V. Tang, Y. Peysson and J. Decker, *Rev. Sci. Instrum.* **77**, 103504 (2006)
[38] N. Bretz, D. Simon, R. Parsells, R. Bravenec, W. Rowan, N. Eisner, M. Sampsell, H. Yuh, E. Marmar, and J. Terry. Review of Scientific Instruments, **72** 1012 (2001).
[39] P. T. Bonoli and E. Ott, *Physics of Fluids* **25**, 359 (1982)

[40] L. L. Lao, H. St John, R. D. Stambaugh, A. G. Kellman, and W. Pfeiffer. Nucl. Fusion, **25** 1611 (1985).

[41] J.E. Rice, A.C. Ince-Cushman, P.T. Bonoli, M.J. Greenwald, J.W. Hughes, R.R. Parker, M.L. Reinke, G.M. Wallace, C.L. Fiore, R.S. Granetz, A.E. Hubbard, J.H. Irby, E.S. Marmar, S. Shiraiwa, S.M. Wolfe, S.J. Wukitch, M. Bitter, K. Hill, and J.R. Wilson. Nucl. Fusion, **49** 025004 (2009).

[42] J. Ko, S. Scott, S. Shiraiwa, M. Greenwald, R. Parker, and G. Wallace. Rev. Sci. Instrum. **81** 033505 (2010).

[43] F. M. Levinton, S. H. Batha, and M. C. Zarnstorff. Review of Scientific Instruments, 68(1):926, 1997.

[44] S. Shiraiwa, J. Ko, O. Meneghini, R. Parker, A. E. Schmidt, S. Scott, M. Greenwald, A. E. Hubbard, J. Hughes, Y. Ma, Y. Podpaly, J. E. Rice, G. Wallace, J. R. Wilson, S. M. Wolfe, and Alcator C.-Mod Group. Phys. Plasmas **18** 080705 (2011).

[45] Petty C.C, Fox W.R, Luce T.C., Makowski M.A. and Suzuki T., Nucl. Fusion **42** (2002) 1124

[46] A. B. Rechester and M. N. Rosenbluth, Phys. Rev. Lett. **40** 38 (1978)

[47] A. E. Schmidt, Measurements and Modeling of Lower Hybrid Driven Fast Electrons on Alcator C-Mod PhD thesis, Massachussets Institute of Technology,

[48] Houlberg WA *et al*, Phys. Plasmas (1997) **4** 3230

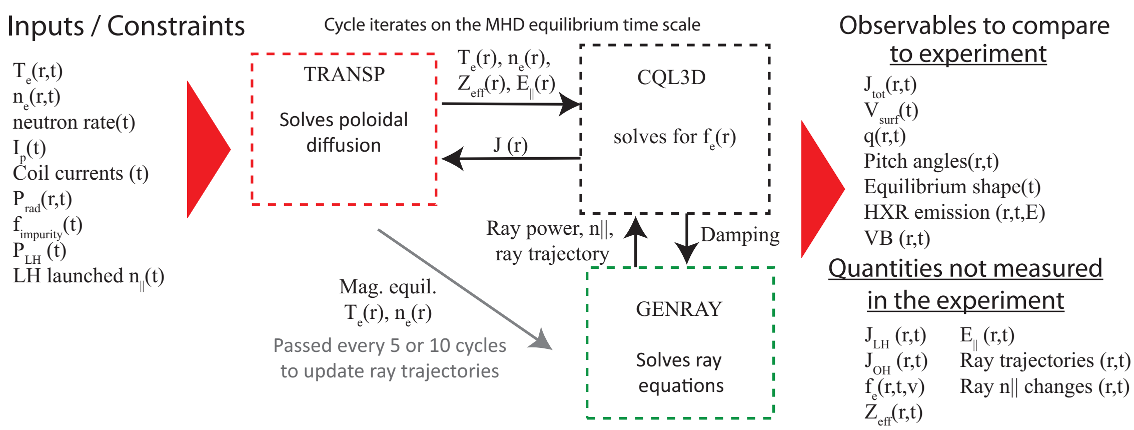

Figure 1. Flow chart for the integration of GENRAY/CQL3D in TRANSP.

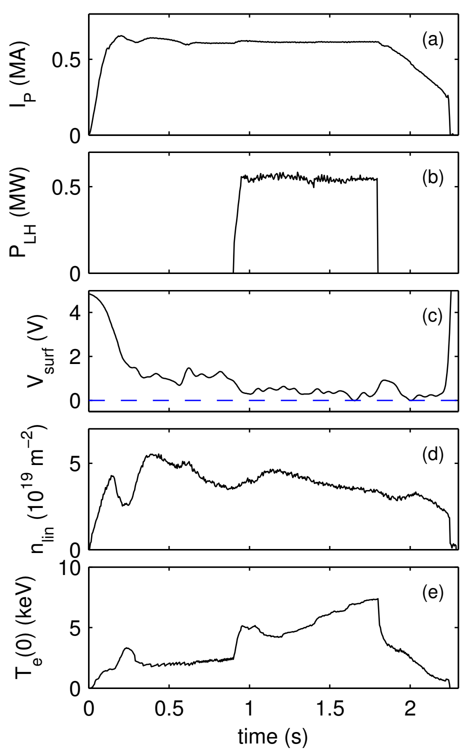

Figure 2. Waveforms for discharge 1120912028. (a) plasma current, (b) LH power coupled to the plasma, (c) surface voltage, (d) line averaged density, (e) central electron temperature from the GPC diagnostic.

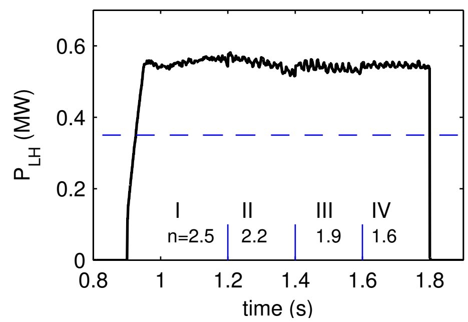

Figure 3. Lower Hybrid power coupled to the plasma. Vertical lines indicate the times at which the antenna phasing is changed, with the values of $n_{\|}$ reported in each time window. Each horizontal line indicates the time windows where measurements from the MSE diagnostic are available. The length of each line (60 ms) represents the integration time of the MSE diagnostic.

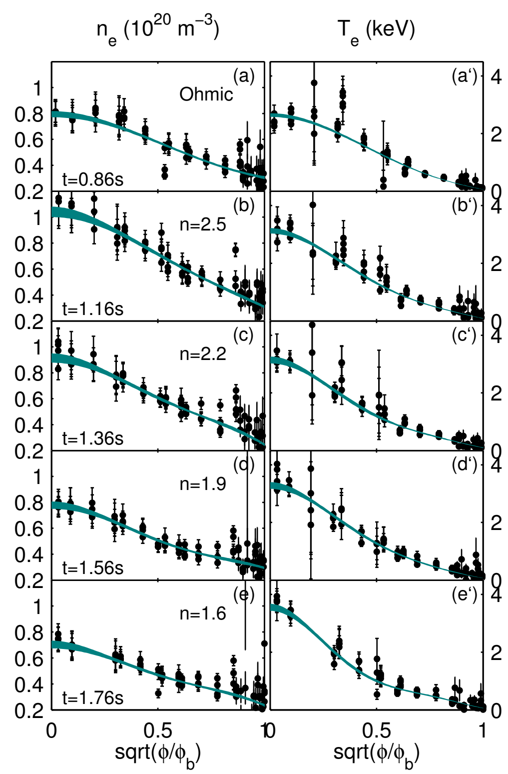

Figure 4. Profiles of electron density (left) and electron temperature (right) from the Thomson scattering (symbols), with superposed the profiles fitted with the GPR technique with their uncertainty region, as a shaded area. Data are fitted over sliding time windows 40 ms wide, to increase statistics, and with separation of 10 ms between consecutive fits.

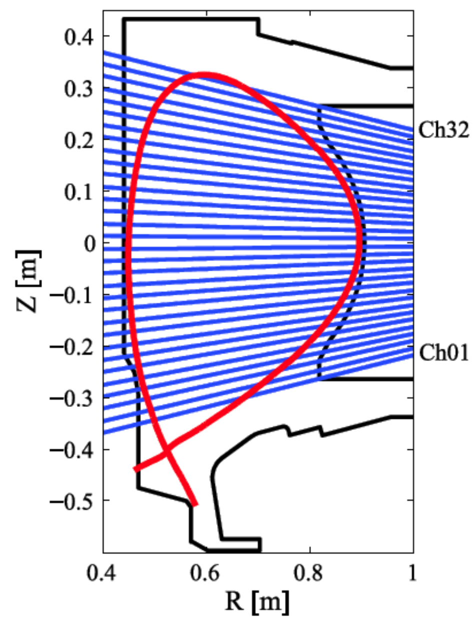

Figure 5. Sketch of the C-Mod plasma cross-section with the line of integrations of the HXR diagnostic chords. Channel 1 looks close to the X-point and channel 32 looks to the top of the plasma.

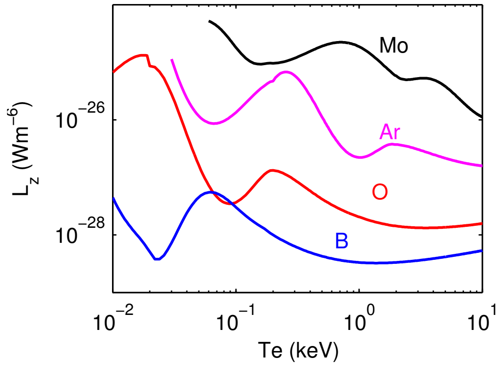

Figure 6. Cooling rates for B, O, Ar and Mo, for temperatures up to 10 keV.

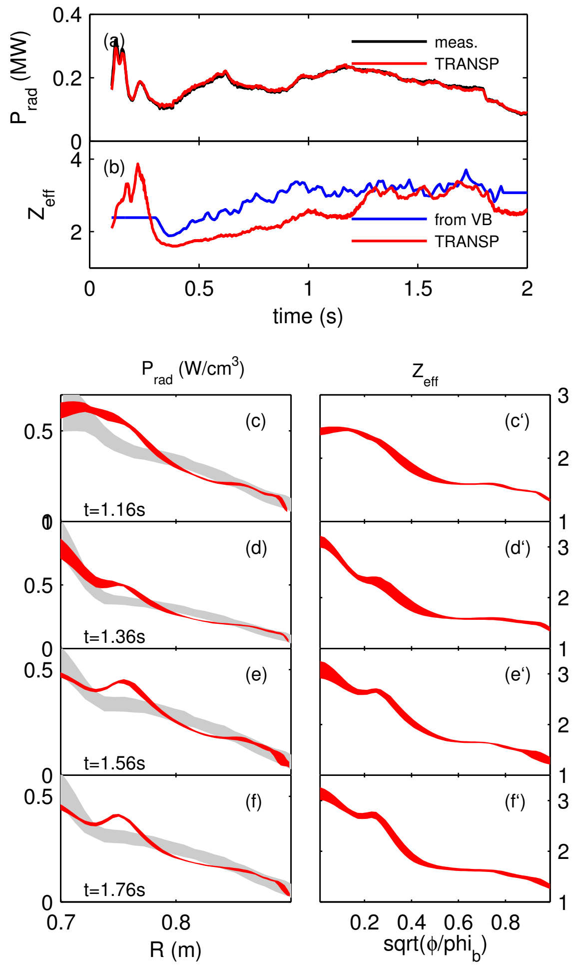

Figure 7. (a) Total radiation measured with the bolometer (black) and calculated in TRANSP (red). (b) Plasma composition Z_{eff} measured (black, rescaled by 0.5), calculated from Visible Bremsstrahlung using eq.3 (blue) and calculated using Eq.4 and TRANSP (red). (c)-(f) profile of radiation power density, comparison between measurements (shaded area) and predictions with TRANSP (red) during the LH phase; the shaded area accounts for systematic errors and for local variations in the time window of interest. (c′)-(f′) profile of Z_{eff} in the same time windows. All profiles are averaged over the integration time of the MSE diagnostic, 60 ms.

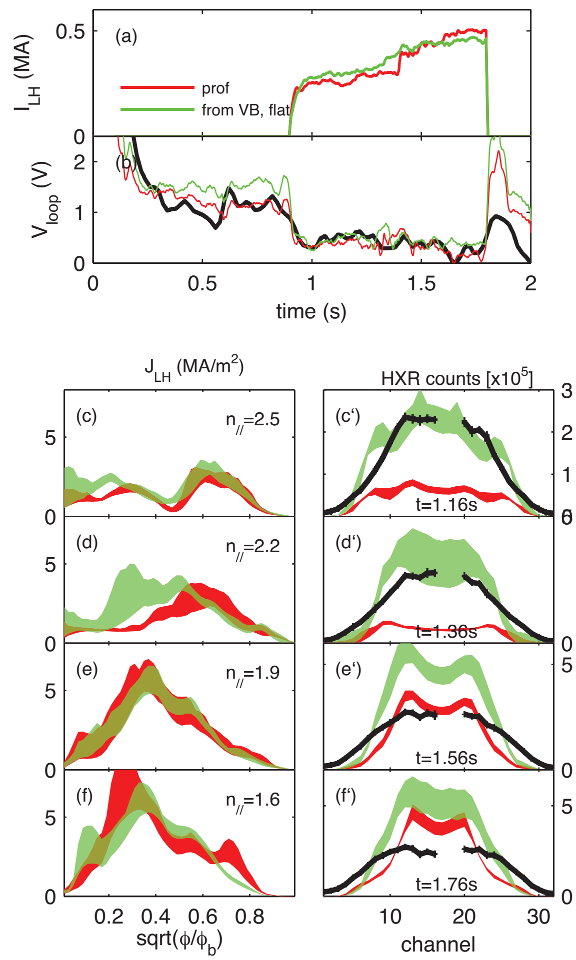

Figure 8. Free-boundary simulations run under two different assumptions on the plasma composition: flat Z_{eff} profiles calculated from Visible Bremsstrahlung and peaked profiles calculated from radiation. (a) LH driven current, (b) surface voltage, compared with the measured value, (c)-(f) LH current density profiles for a flat Z_{eff} input profile (green) and for a shaped Z_{eff} profile (red), (c$'$)-(f$'$) measured HXR profiles (black) and synthetic diagnostic profiles for a flat Z_{eff} profile (green) and for a shaped Z_{eff} profile (red). All profiles are averaged over a time window of 60 ms.

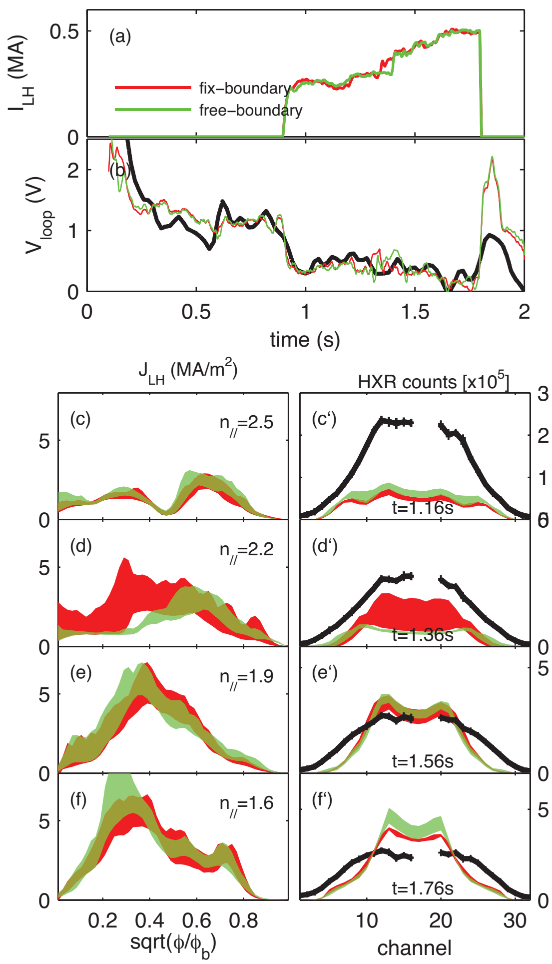

Figure 9. (a) Lower hybrid driven current calculated with the fixed-boundary equilibrium solver TEQ (red) and with the free-boundary Isolver (green). (b) surface voltage measured (black) and calculated with TEQ (red) and with Isolver (green). (c)-(f) LH current density profiles averaged over 60 ms (c′)-(f′) HXR emissivity profiles, measured (black) and simulated with CQL3D, same color coding as in (a) and (b).

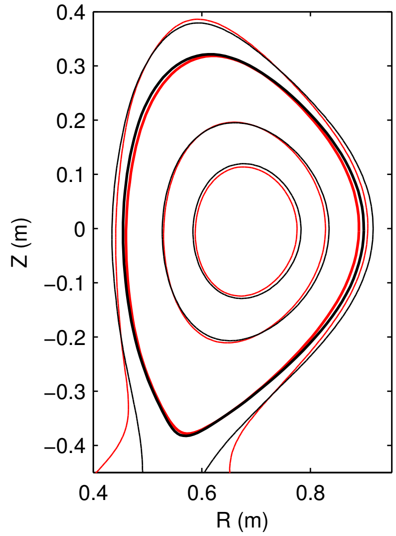

Figure 10. Comparison between fix-boundary (black) and free-boundary (red) simulations. Also shown are the plasma boundary and the flux surfaces at $\sqrt{(\phi/\phi_b)} = 0.3$ and 0.6 and the surfaces outside the separatrix, at $\sqrt{(\phi/\phi_b)} = 1.1$.

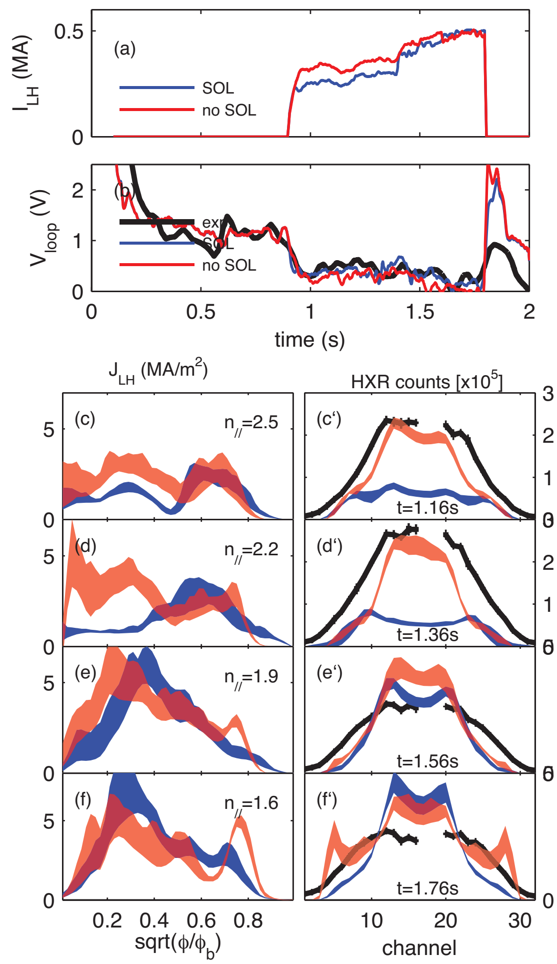

Figure 11. Comparison of simulations with and without SOL in GENRAY. (a) integrated LH current (b) surface voltage (c)-(f) LH current density profiles (c')-(f)' HXR emissivity profiles.

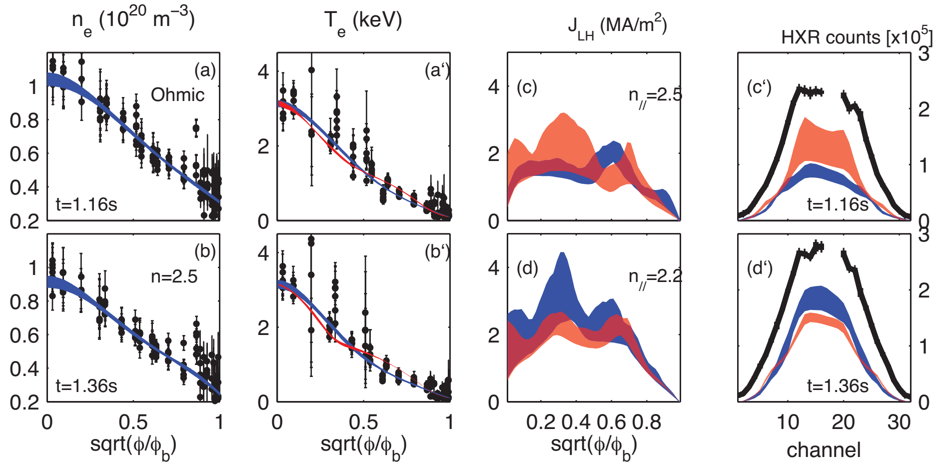

Figure 12. Left panel: measured profiles of electron density and temperature from the Thomson Scattering in a time window of 60 ms centered at 1.16 s (top) and at 1.36 s (bottom). The blue-shaded area indicates the input profiles to TRANSP in the same time window, the red-shaded area indicates input profiles where the electron temperature in the outer mid-radius has been artificially increased and the temperature in the inner mid-radius decreased. Right panel: range of variation of the lower hybrid current density profiles and of the HXR profiles in the same time windows.

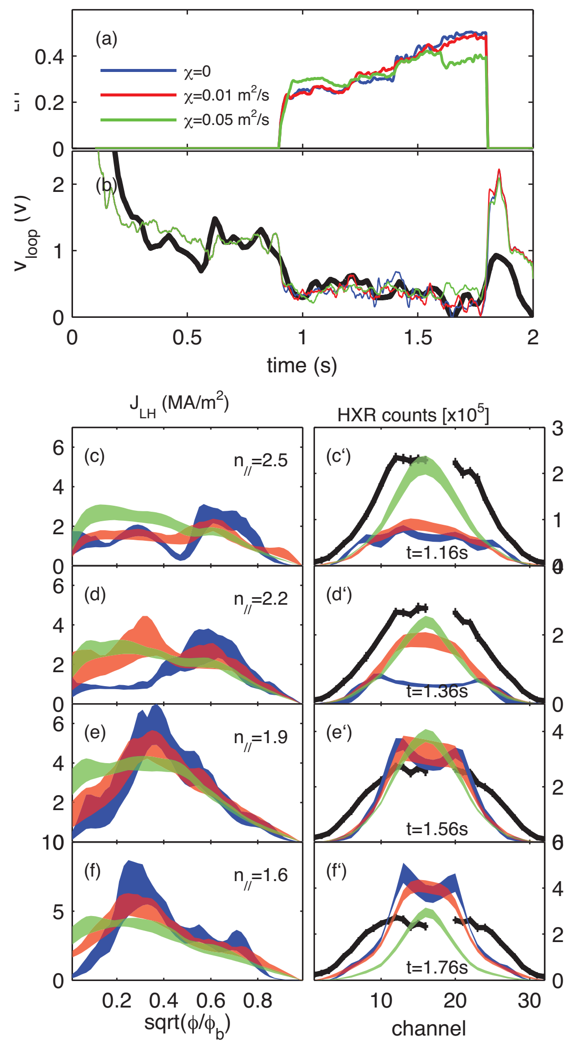

Figure 13. Simulations run under different assumptions on the radial diffusion: no radial diffusion ($\chi_0 = 0$) and two values of diffusion $\chi_0 = 0.01$ m^2/s and $\chi_0 = 0.05$ m^2/s. (a) LH driven current, (b) surface voltage, compared with the measured value, (c)-(f) LH current density profiles for the three values of χ_0, same colors as in (a). (c$'$)-(f$'$) measured HXR profiles (thick black) and synthetic diagnostic profiles for the three values of χ_0, same colors as in (a). All profiles are averaged over a time window of 60 ms.

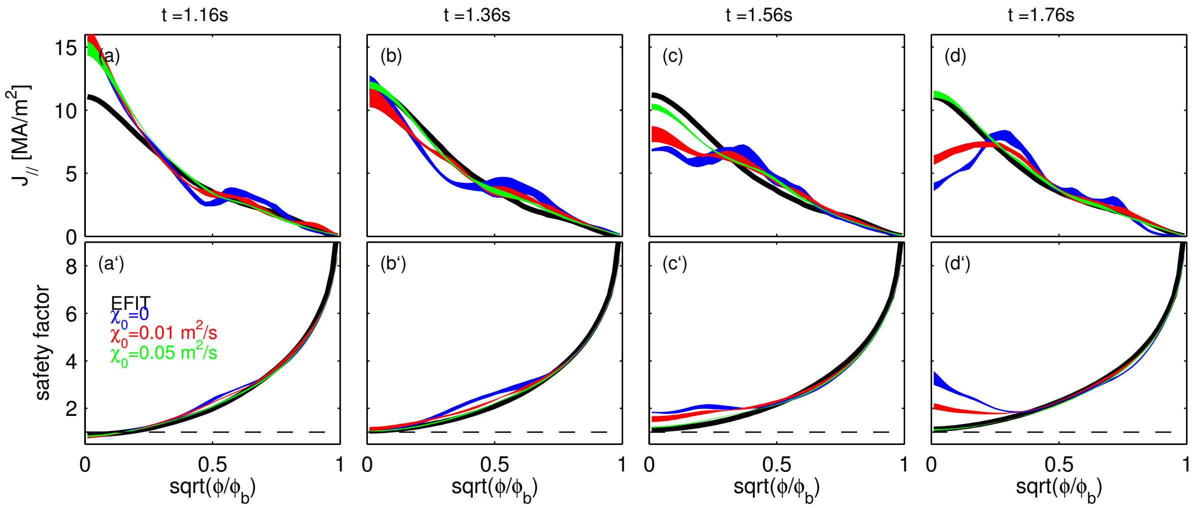

Figure 14. Plasma current profiles (top) and safety factor profiles (bottom), constrained from the MSE diagnostic (black) and calculated with free-boundary TRANSP in the absence of radial diffusion ($\chi_0 = 0$, blue) and for two assumptions on the anomalous radial diffusion coefficient: $\chi_0 = 0.01$ m^{2}s^{-1} (red) and for $\chi_0 = 0.05$ m^{2}s^{-1} (green). All calculated profiles are averaged over 60 ms and the shaded area indicates the variation in the selected window, centered at the time where the EFIT profiles are available.

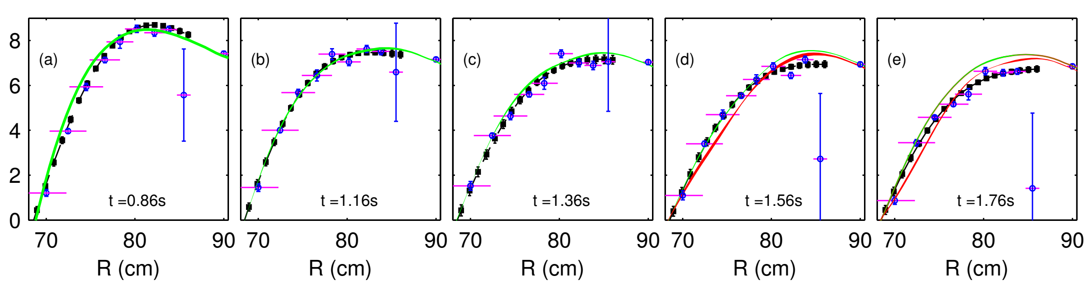

Figure 15. Magnetic pitch angle. Measured values (blue) in the time windows reported. Vertical bars represent experimental errors. The point at 90 cm is from magnetic measurements and is used as a constraint in the EFIT reconstruction. Horizontal magenta lines indicate the radial region of measurement of the MSE. Black symbols indicate the interpolated points that go into EFIT. The green and red shaded areas represent the pitch angle calculated from the magnetic equilibrium evolved in TRANSP and averaged over 60ms, for $\chi_0 = 0.05$ m^{2}s^{-1} and $\chi_0 = 0.01$ m^{2}s^{-1} respectively. Color coding for the diffusion coefficients is the same as in Fig.13 and Fig.14.

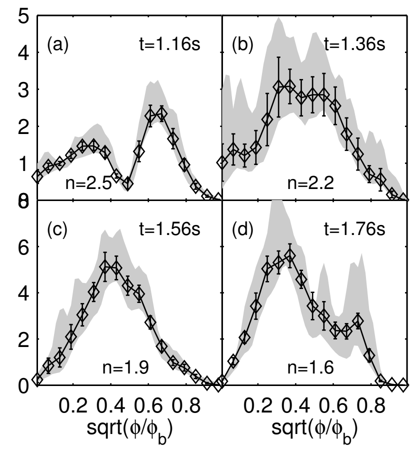

Figure 16. Lower hybrid current density profiles, calculated with GENRAY+CQL3D. The shaded area indicates the range of variation of the calculated current for variations of the input parameters in CQL3D and GENRAY, such as the mesh resolution in velocity space, the integration time in CQL3D for the calculation of the distribution function and number of internal steps. The curves with error bars correspond to the reference simulation, run with 400 mesh points in the velocity space, 0.4 ms integration time and 5 time steps.

“Experimental and modeling uncertainties in the validation of lower hybrid current drive”

Submitted by

F. M. Poli, J. R. Wilson, R. Andre, S. Scott, L. Delgado-Aparicio, (PPPL)
P. T. Bonoli, M. Chilenski, R. Mumgaard, S. Shiraiwa, G. M. Wallacem J. RiceI. Faust, R. Granetz, J. Hughes, J. Walk (PSFC, MIT), M. Reinke (ORNL), R.H. Harvey, Yu. Petrov (CompX)

fpoli@pppl.gov

03/14/2016

Princeton Plasma Physics Laboratory

Princeton Plasma Physics Laboratory
Office of Reports and Publications

Managed by
Princeton University

under contract with the
U.S. Department of Energy
(DE-AC02-09CH11466)

P.O. Box 451, Princeton, NJ 08543
Phone: 609-243-2245
Fax: 609-243-2751
E-mail: publications@pppl.gov
Website: http://www.pppl.gov